2d Quantifying the effectiveness of rolling dynamic compaction using FEM-SPH coupling method

Y. Chen, J. Xue
School of Engineering and IT, University of New South Wales, Canberra, Northcott Road, Campbell 2612, Australia, yue.chen4@adfa.edu.au

M.B. Jaksa, B.T. Scott, Y.L. Kuo
School of Architecture and Civil Engineering, University of Adelaide, SA 5005, Australia

ABSTRACT: Rolling dynamic compaction (RDC) is a soil improvement technique, which has been successfully applied to many construction projects. Compared with conventional rollers, RDC has the ability to improve the ground more effectively and efficiently since it has a greater depth of influence and higher travel speeds. This paper presents a three-dimensional finite element method (FEM)-smoothed particle hydrodynamics (SPH) model which simulates the soil response and soil-roller interactions during the RDC process. The developed FEM-SPH model was compared against results obtained from a field study and experimental tests. Parametric studies were also performed to determine their influences on the effectiveness of RDC. The results of this study demonstrate the capability of the FEM-SPH model to simulate the ground improvement induced by RDC.

KEYWORDS: Ground improvement, FEM-SPH coupling method, SPH, rolling dynamic compaction

1 INTRODUCTION

Rolling dynamic compaction (RDC) is a specific form of dynamic compaction, which has been used for soil densification over the past few decades. It consists of towing heavy (6–15 tonnes), non-circular (3-, 4- and 5-sided) modules behind a tractor. During operation, the modules rotate and fall to impact the ground. Compared to conventional circular drum rollers, which operate at a typical speed of 4 km/h (Pinard, 1999), RDC can achieve greater speeds (10–12 km/h), while also improving the ground at deeper depths (1–3 m) due to its larger module mass and its ability to deliver both kinetic and potential energies to the ground during the compaction process. Therefore, RDC has been successfully and extensively applied in a wider range of earthworks construction, such as, in situ densification of existing fills, large reclamation projects, reconstruction of rural roads and mining and agricultural related applications (Avalle & Carter, 2005, Avalle & McKenzie, 2005, Bouazza & Avalle, 2006).

Previous researchers have studied the effectiveness of RDC using different techniques, such as, field tests (Avalle & Carter, 2005, Scott & Jaksa, 2014, Bradley et al., 2019, Scott et al., 2019, 2020), experimental scale model tests (Rajarathnam et al., 2016, Chung et al., 2017, Chen et al., 2022), numerical modelling (Kuo et al., 2013, Chen et al., 2021a, b) and programming (Ranasinghe et al., 2017a, b, 2019). In the numerical models developed by Kuo et al. (2013) and Bradley et al. (2023), both the soil and the roller were simulated using the finite element method (FEM). Ground settlements and influence stresses predicted by the FEM model at static and dynamic loadings were compared against field data. It was reported that, the FEM model is capable of simulating the soil responses under the impact roller. Due to the continuum nature of the FEM, the main disadvantage of the developed FEM model is that the motion of soil particles during the compaction process is difficult to be simulated. Therefore, the discrete element method (DEM) was adopted by Chen et al. (2021a) and Chen et al. (2021b) to simulate the soil using a large number of particles. Given the particulate nature of the DEM, soil displacements induced by the roller are able to be tracked at each time step, which provides detailed information on soil movements. For example, the velocity vectors of soil particles with respect to the motion of the roller were reported by Chen et al. (2021b) to help understand the soil displacement pattern under the roller. The velocity vectors of soil particles were also employed by Chen et al. (2021a) to infer the depth of major improvement of the roller. Although the DEM provides a greater understanding of the behaviour of soil particles under the roller at the microscopic scale, it has higher requirements on the computational resources. As reported by Chen et al. (2021a), one RDC simulation, consisting of 25 passes and approximately 54,000 particles, typically took approximately 30 days to run using a supercomputer with 12 CPU cores (2 × Intel Xeon Gold 6248 Processor @2.4 GHz). It can be seen that, although the DEM provides a greater understanding of the behaviour of soil particles under the roller at a microscopic scale, it is computationally expensive and therefore may be difficult to apply to simulate large-scale problems or for industrial applications. To overcome the limitations of the FEM and the DEM, the smoothed particle hydrodynamics (SPH) method is adopted in this paper to simulate the soil response under the roller.

The SPH is a continuum-based, mesh-free method, which was originally introduced to study astrophysical problems by Lucy (1977) and Gingold & Monaghan (1977). Instead of using a grid or mesh, particles are employed in the SPH model. However, unlike the particles used in the DEM, which represent actual individual particles, the particles used in the SPH represent discrete volumes of the computational domain. Therefore, compared with the FEM and the DEM, the SPH has the ability to model the dynamic characteristics of the problem with greater computational efficiency. Due to its ability in modelling problems related to discrete particles with large deformations, the SPH has been adopted by many researchers to simulate the behaviour of soil in studying geotechnical engineering related problems (El-Gindy et al., 2011, Gheshlaghi et al., 2021, Wang et al., 2021).

Since the SPH combines the advantages of both the FEM and the DEM, in this study, a new numerical model is developed to simulate soil responses under the Broons BH-1300 4-sided, 8-tonne roller. The soil is modelled using the SPH and the roller is simulated by the FEM. Results of the developed model are validated against the field measurements and experimental test results. Parametric studies are performed using the proposed SPH model to provide a greater understanding of the influences of these parameters on the effectiveness of RDC.

2 FIELD STUDY

A field study was undertaken by Scott et al. (2016) using the BH-1300, 4-sided, 8-tonne impact roller at Monarto Quarries, Callington, South Australia. The field trial was performed on a

test pad, which was excavated to 1.5 m depth and then backfilled with improved crushed rock quarry material. The fill material was classified as a well-graded Sandy Gravel (GW) in accordance with the Unified Soil Classification System. The field particle size ranges between 0.07 and 10 mm, with D_{50} of 2 mm. The test pad had a length of 4 m, and two earth pressure cells (EPCs) were buried at 0.7 and 1.1 m depths below the ground surface to measure pressures induced by RDC. Ground settlements were measured after every 2 roller passes until pass 10, and then every 5 passes thereafter until pass 80. The average initial dry density of the soil was approximately 1725 kg/m^3. The roller was operated at a constant traveling speed of 11 km/h during the field study.

3 NUMERICAL MODEL DEVELOPMENT

A three-dimensional numerical model is developed using the commercial software LS-DYNA (LSTC, 2018) in this study. As shown in Figure 1, the numerical model consists of the roller, the soil mass, and a base. The base is simulated using the FEM and it is used to facilitate the motion of the roller when multiple roller passes are performed. The base is fixed at its initial location with no movement or deformation permitted during the compaction process. The sides of the base, which contact with the soil mass, are set as non-reflecting boundaries. The roller is also modelled using the FEM as a rigid body with dimensions of 1495 × 1495 × 1300 mm (height × length × width). According to Kuo et al. (2013), the roller is effectively rigid relative to the stiffness of the underlying soil and hence, the deformation of the roller during compaction is negligible. The horizontal speed of the roller is specified in the numerical model and in this study; a value of 11 km/h is adopted. The effect of the spring-linkage system on the 4-sided roller is modelled as an equivalent spring according to Scott et al. (2020). The vertical speed of the roller is not constrained and is calculated by the numerical model based on the horizontal and rotational speeds of the roller, the conditions of the underlying soil, and the undulating surface compacted by the previous roller pass.

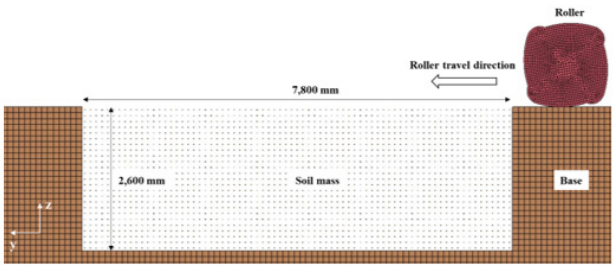

Figure 1. Numerical model setup.

The soil mass is simulated using the SPH with dimensions of 7800 × 2600 × 2600 mm (length × width × height). As mentioned above, the computational domain is discretised into a set of particles in SPH, and the field variables (velocity, acceleration, density, and pressure/stress) are carried by the particles. The approximation of the field variables in the computational domain is obtained using two basic steps, namely the kernel approximation and the particle approximation. The kernel approximation involves the continuous integral representation of a function variable g and its derivatives in the influence domain Ω using a smoothing function $W(x-x',h)$, as shown in Equation (1). A variety of smoothing functions has been developed and used by many researchers. A detailed discussion of the available smoothing functions is given by Liu & Liu (2010). In this study, the most commonly adopted cubic B-spline smoothing function [Equation (2)] is used.

$$g(x) \approx \int_\Omega g(x')W(x-x',h)dx' \tag{1}$$

where x is the coordinate vectors of the particle; x' is the coordinate vectors of any particle within the influence domain; and h is the smoothing length which varies with time.

$$W(x-x',h) = a_d \times \begin{cases} \frac{2}{3} - d^2 + \frac{1}{2}d^3, 0 \le d < 1 \\ \frac{1}{6}(2-d)^3, 1 \le d \le 2 \\ 0, \quad d \ge 2 \end{cases} \tag{2}$$

where a_d is $\frac{1}{h}$, $\frac{15}{7\pi h^2}$ and $\frac{3}{2\pi h^2}$ in one-, two- and three-dimensional space; and d is the distance between particles x and x'.

The second step is particle approximation, which involves discretising the continuous integral representation as a summation of these values over the neighbouring particles (Liu & Liu, 2010). As shown in Equation (3), the particle approximation of $g(x)$ can be expressed as:

$$g(x) \approx \sum_{j=1}^{M} \frac{m_j}{\rho_j} g(x_j) W(x-x_j,h) \tag{3}$$

where m_j and ρ_j are the mass and density of particle j, respectively; and M is the total number of particles within the influence area at x.

The interaction between the FEM and the SPH is treated using the penalty-based contact algorithm in LS-DYNA (LSTC, 2018). Particles used in the SPH approach are checked for penetration through the contact surface of the finite elements. If penetration is detected, the contact forces are applied to the interface between the penetrated SPH particles and the finite element nodes, which are calculated based on the penetration depth and the contact stiffness.

3.1 *Soil constitutive law*

Considering the nonlinear behaviour of soil during the RDC compaction process, the cap model is adopted as the soil constitutive law to simulate the soil response in this study. This model has been successfully used to simulate soil behaviour under dynamic compaction in previous studies (Zhou et al., 2020, Yao et al., 2022, Zhou et al., 2022). As shown in Figure 2, the extended cap model has three surfaces, which are the failure envelope (f_1), the cap surface (f_2), and the tension cutoff (f_3), in the $\sqrt{J_{2D}} - J_1$ plane. J_1 and J_{2D} represent the first invariant of the stress and the second invariant of the deviatoric stress tensor, respectively. A detailed description of the theories associated with the cap model is given by LSTC (2018). The three surfaces of the cap model are defined by Equations (4)–(6), respectively.

$$f_1 = \sqrt{J_{2D}} - \alpha + \gamma \exp(-\beta J_1) - \theta J_1 \tag{4}$$

$$f_2 = \sqrt{J_{2D}} - \frac{1}{R}\sqrt{[X(k) - L(k)]^2 - [J_1 - L(k)]^2} \tag{5}$$

$$f_3 = T - J_1 \tag{6}$$

where α, γ, β and θ are the material parameters of the failure surface; R is the curvature of the hardening cap; T is the maximum hydrostatic tension; and k is the hardening parameter related to the actual plastic volumetric change ε_v^p and ε_v^p which is given by:

$$\varepsilon_v^p[X(k)] = W\{1 - exp[-D(X(k) - X_0]\} \tag{7}$$

where W, D and X_0 are the material parameters, and X_0 is the initial value of the cap parameter $X(k)$.

According to Zhou et al. (2020), the parameters α and θ used in Equation (4) can be calculated using the internal friction angle (ϕ) and cohesion (c) obtained from consolidated drained triaxial test results as follows:

$$\alpha = \frac{6 \cdot c \cdot \cos\phi}{\sqrt{3}(3 - \sin\phi)} \tag{8}$$

$$\theta = \frac{2\cdot\sin\phi}{\sqrt{3}(3-\sin\phi)} \quad (9)$$

In this study, the value of the maximum hydrostatic tension, T, is assumed to be zero since the soil is under compression during the RDC compaction process. The values of γ and β are assumed to be zero to convert the curved failure envelope f_1 to a linear failure surface. The parameter X_0 is the initial cap position on the J_1 axis, with larger values of X_0 indicating higher pressures required to compress the soil. In this study, before the compaction commences, there are no additional forces imposed on the soil, therefore, it is reasonable to assume that the vertical stress of the soil at a given point is only due to the weight of the soil above that point. Based on the horizontal and vertical stresses of soil near the depth of 2600 mm (the bottom of the soil body) obtained from the numerical model, X_0 equals 81 kPa. Therefore, there are five parameters in the cap model that need to be calibrated, which are α, θ, W, D and R.

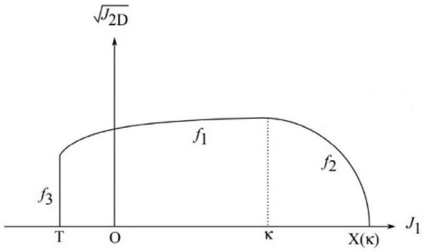

Figure 2. The yield surface of the extended two-invariant cap model in $\sqrt{J_{2D}} - J_1$ plane (LSTC, 2018).

3.2 *Model parameters*

Consolidated drained triaxial and oedometer tests were performed to obtain the geotechnical properties of the soil. The ϕ and c derived from the triaxial test results are 29.6° and 8.8 kPa, respectively, and the values of α and θ are then calculated using Equations (8) and (9). Other parameters used in the cap model are calibrated using the obtained consolidated drained triaxial and oedometer test results. The cap model input parameters are shown in Table 1.

Table 1. The cap model input parameters.

Mass density (t/mm^3)	1.725E-9
Initial bulk modulus (MPa)	44.3
Initial shear modulus (MPa)	20.5
α (MPa)	0.0105
θ	0.228
R	4.39
D (MPa^{-1})	0.05
W	0.34

The initial spacing of SPH particles is an essential parameter in determining the accuracy and efficiency of the numerical model. As shown in Equation (2), the initial smoothing length relates to the initial distance between the SPH particles, which affects the computational time of the numerical model. Smaller SPH particle initial spacing increases the accuracy of the model but also increases the simulation running time. Therefore, it is important to select the appropriate particle initial spacing. In addition, a constant particle initial spacing in all directions is recommended to ensure the stability of the model (Bojanowski, 2014). Four numerical tests, with particle initial spacing equal to 52, 104, 200, and 325 mm, were performed up to two roller passes to examine the optimum particle initial spacing. Other parameters were kept constant in these four tests.

Table 2 presents the required simulation running time for each particle initial spacing. Although the running time decreases significantly, when the particle initial spacing increases to 325 mm, it was observed from the model results that the motion of the roller is affected by such a large particle spacing. As shown in Figure 3a, when the roller rotates about its corner, due to the large spacing of the particles, the corner of the roller drops below the soil located at the ground surface, which results in unstable roller motion. When the particle spacing decreases to 200 mm, the motion of the roller becomes stable. However, the corner of the roller in Figure 3b is still slightly below the ground surface. This phenomenon is further improved when the spacing equals 104 mm (Figure 3c), and no significant improvement is observed when the particle spacing reduces to 52 mm (Figure 3d). In addition, the simulation running time increases to 24 hours for a 52 mm spacing, compared with the required 9.2 hours for a 104 mm spacing. Therefore, the optimum particle initial spacing is selected to be 104 mm to optimise computational time and ensure a stable motion of the roller. A total of 30 roller passes with a 104 mm particle initial spacing were performed in the numerical simulation on a supercomputer (2 × Intel Xeon Gold 6248 Processor @2.4 GHz) using the ANSYS (LS-DYNA) software.

Table 2. Required simulation running time.

Particle initial spacing (mm)	52	104	200	325
Simulation running time (hours)	24	9.2	5.9	3.3

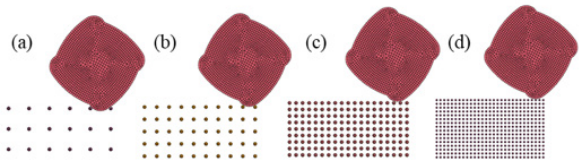

Figure 3. The motion of the roller with respect to different particle initial spacing: (a) 325 mm, (b) 200 mm, (c) 104 mm, (d) 52 mm.

4 MODEL VALIDATION

4.1 *Comparison between the SPH model and field study*

Ground settlement is often considered as an important indicator of soil improvement induced by RDC, since measuring ground settlement is relatively efficient and requires less testing equipment compared to other in situ testing methods, such as nuclear density tests, dynamic cone penetration tests, cone penetration tests, and seismic surface wave techniques. Therefore, ground settlements obtained from the numerical model are compared against those measured by the field tests. In the field tests, ground settlement was measured by surveying the ground surface imparted by the roller, and the readings were taken after every 2 roller passes up to pass 10 and then every 5 passes thereafter. Ground settlement was obtained by tracking the movement of the SPH particles during RDC compaction in the numerical model.

Figure 4 plots ground settlements with respect to the number of passes from the numerical model and the field tests. It can be seen that ground settlement increases with an increasing number of passes, and the rate of change in ground settlement diminishes with the number of passes. Two trend lines are drawn to fit the numerical results and field measurements. In general, the shape of these two trend lines is similar, which indicates that the numerical ground settlements are in broad agreement with the measured results from the field study. Ground settlements after 30 roller passes predicted by the numerical model and measured in the field trial are approximately 96.8 and 107.2 mm, respectively. Therefore, it can be concluded that the numerical model is able to provide reasonable predictions of ground settlements induced by the roller.

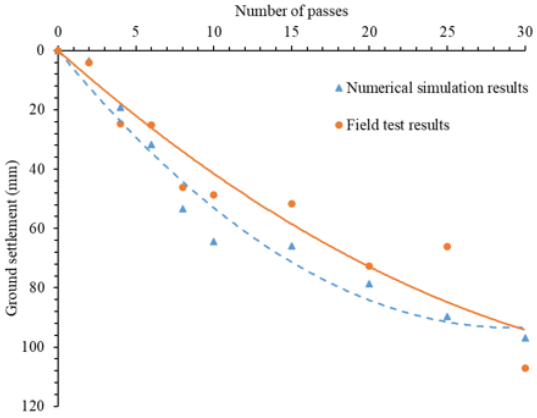

Figure 4. Ground settlements obtained from the numerical model and field tests.

4.2 Comparison between the SPH model and experimental tests

The soil displacement pattern at the centreline of the roller obtained from the SPH model is compared against that reported by Chen et al. (2022) from experimental tests, as shown in Figure 5. In Chen et al. (2022), soil displacements were measured from the movement of a one-particle thick layer of dyed fused quartz located along the centreline of the traverse of the roller, using a high speed digital camera and the particle image velocimetry (PIV) technique. Subsets, with a diameter of approximately 25 mm, were used in the PIV analysis. Therefore, each soil displacement vector displayed in Figure 5b represents the average displacement of soil particles located within that subset. This is similar to the soil displacement vectors measured from the SPH model (Figure 5a), where each SPH particle represents a portion of the computational domain (in this study, the soil mass). It is worth mentioning that the roller used by Chen et al. (2022) is the 1:13 scale model of the 4-sided, 8-tonne impact roller with dimensions of 115 × 115 × 100 mm (height × length × width), and a weight of 3.64 kg. Therefore, the scales used in Figures 5a and 5b are different. In addition, the operating speed of the roller in the numerical model is 11 km/h, while the scaled roller in Figure 5b travelled at a speed corresponding to 12 km/h.

It can be seen from Figures 5a and 5b that the soil beneath the roller is compacted and displaces downwards. As the roller travels from right to the left in both Figures 5a and 5b, the soil is also pushed and displaces in the lateral direction of the roller's motion. Soil displacement vectors from Chen et al. (2022) show more obvious horizontal displacements than those predicted by the numerical model. This discrepancy can be explained by the different properties of the soil and different roller operating speeds used in the experiments and the numerical model.

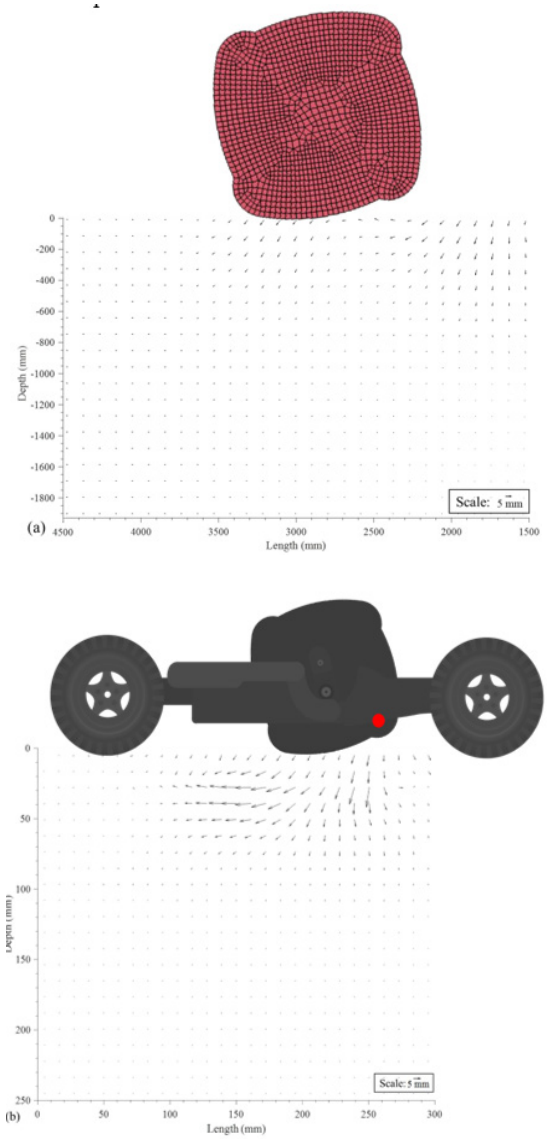

Figure 5. Soil displacement vectors: (a) from the SPH model, (b) from Chen et al. (2022).

5 PARAMETRIC STUDY

5.1 *Roller weight*

In addition to the 8-tonne impact roller, Broons also manufactures and operates a heavier version of the 4-sided roller, which weighs 12 tonnes (BH-1300HD). Therefore, in this study, the effect of module weight on the ground improvement results is investigated using the developed numerical model. The roller mass was increased to 12 tonnes and other inputs remained constant in the model. The simulation was performed up to 15 passes. Figure 6 presents ground settlement results for both the 8- and 12-tonne rollers. As one would expect, the 12-tonne roller produces greater ground settlements when compared with those induced by the 8-tonne roller. Figure 6 also suggests that the 12-tonne roller is able to achieve similar soil improvement results as those of the 8-tonne roller with greater efficiency, since fewer passes are required for the 12-tonne roller.

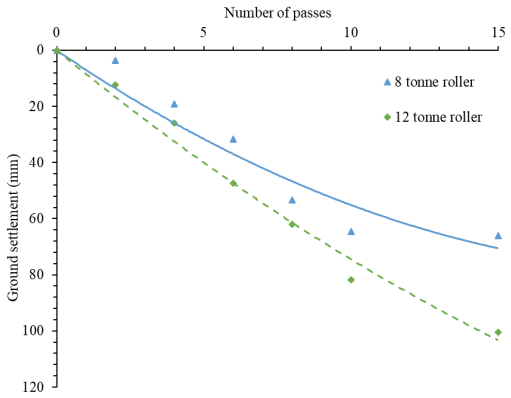

Figure 6. Ground settlements induced by 8- and 12-tonne rollers.

In addition to ground settlement, velocity vectors of SPH particles are also plotted to examine soil movements under the 8- and 12-tonne rollers, since velocity vectors directly reflect the response of the soil induced by RDC. As shown in Figure 7, the overall soil displacement pattern induced by the 8-tonne roller is similar to that of the 12-tonne roller. Compared with the 8-tonne roller, the 12-tonne roller results in greater soil movements as evidenced by the larger velocity vectors under the roller in Figure

7b. Greater velocity vectors observed at deeper depths and greater distances from the contact point between the roller and the soil indicate that the 12-tonne roller has a greater influence zone. In general, based on the numerical results, the heavier roller induces greater soil improvements at higher efficiency. However, there are also several other factors that need to be taken into consideration when deciding whether the 8- or 12-tonne roller would be used in practice. For example, the heavier roller induces greater vibrations to the ground, which can be problematic if the construction site is close to infrastructure. In such cases, continuous vibration monitoring of the ground is required to determine appropriate safe distances for which the roller can be operated without inducing potential hazards to the nearby buildings.

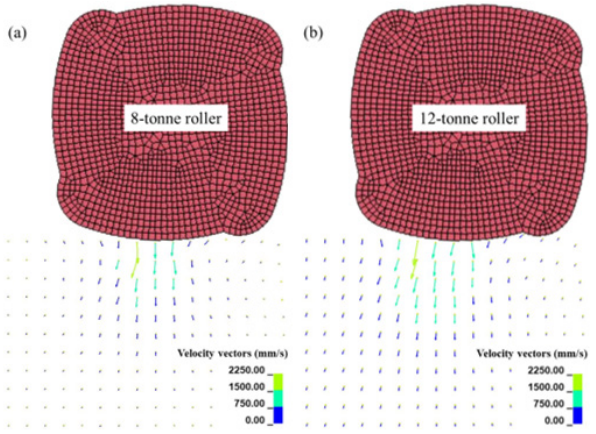

Figure 7. Velocity vectors of SPH particles just after the module's impact: (a) 8-tonne roller, (b) 12-tonne roller.

5.2 *Operating speed*

The influence of operating speed on the effectiveness of the roller is also assessed in this study. The speed of the roller was increased to 13 km/h and other inputs remained constant in the model. Figure 8 presents ground settlements measured in the numerical model when the roller is operated at 11 and 13 km/h. Ground settlements increase as the operating speed rises. However, a faster operating speed does not always yield greater soil improvement. As reported by Clifford (1980) and Scott et al. (2020), there is an upper limit of roller operating speed and the roller will start to skip on the ground and result in inadequate delivery of energy to the ground if the travelling speed is too fast. In addition, a higher operating speed is difficult to be maintained if the construction site is small or restricted. Therefore, it is recommended to conduct field trials to determine the appropriate operation of RDC before commencing actual projects. It is noted that, due to computational and time constraints, only 13 km/h was adopted in the simulation in comparison with the 11 km/h speed. In future work, a range of operating speeds will be investigated to provide a detailed comparison of the soil improvement results induced by different roller speeds.

6 CONCLUSIONS

This paper presents a three-dimensional FEM-SPH model developed using LS-DYNA to investigate the performance of the 4-sided, 8-tonne, Broons BH-1300 impact roller. The roller was simulated using the FEM and the soil was modelled by the SPH. The numerical model was compared and validated against a field trial that was conducted using the same impact roller on the same soil properties. Ground settlements predicted by the numerical model were in good agreement with the field data. The soil displacement pattern obtained from the numerical model was also compared against that measured in experiments and it was found that the numerical model predicts well the soil displacement pattern under the roller. Therefore, it was concluded that, the numerical model provides reasonable predictions of ground improvements induced by RDC.

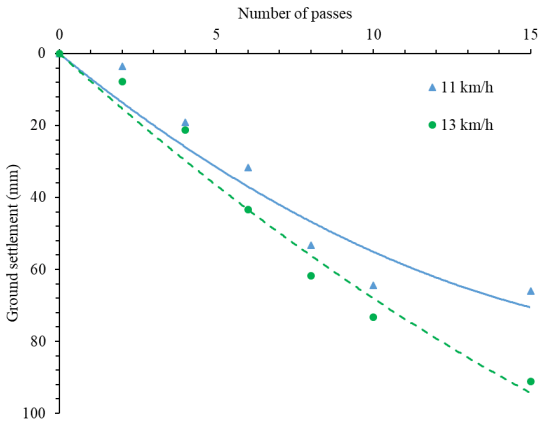

Figure 8. Ground settlements induced by the 8-tonne roller travelling at 11 and 13 km/h speeds.

A preliminary parametric study was then performed using the proposed numerical model to examine the effects of the roller's weight and operating speed on the effectiveness of RDC. The results indicated that the heavier roller produces greater soil displacements and has a larger influence zone, and a higher operating speed results in larger ground settlements. However, the operating speed also affects the motion of the roller, which requires further investigation. In general, the results of this study suggest that the soil response under RDC can be well simulated using the SPH method. Future work will extend this model by examining the influences of operating speed on the motion of the roller and also explore the effectiveness of different RDC modules.

7 ACKNOWLEDGEMENTS

The authors wish to acknowledge the University of Adelaide for access to the Phoenix high performance computing resources.

8 REFERENCES

Avalle, D. and Carter, J. 2005. Evaluating the improvement from impact rolling on sand. *Proc. 6th Int. Conf. on Ground Improvement Techniques*, Coimbra, Portugal, 8pp.

Avalle, D. L. and Mckenzie, R. W. 2005. Ground improvement of landfill site using the square impact roller. *Australian Geomechanics*, 40, 15-21.

Bojanowski, C. 2014. Numerical modeling of large deformations in soil structure interaction problems using FE, EFG, SPH, and MM-ALE formulations. *Archive of Applied Mechanics*, 84, 743-755.

Bouazza, A. and Avalle, D. L. 2006. Effectiveness of rolling dynamic compaction on an old waste tip. *ISSMGE 5th International Congress on Environmental Geotechnics*, Cardiff, 1.

Bradley, A. C., Jaksa, M. B. and Kuo, Y.L. 2019. Examining the kinematics and energy of the four-sided impact roller. *Proceedings of the Institution of Civil Engineers - Ground Improvement*, 172, 297-304.

Bradley, A.C., Jaksa, M.B. and Kuo, Y.L., 2023. Finite element modelling of rolling dynamic compaction. *Computers and Geotechnics*, 157, p.105275.

Chen, Y., Jaksa, M., Kuo, Y. and Scott, B. 2021a. Discrete element modelling of the 4-sided impact roller. *Computers and Geotechnics*, 137.

Chen, Y., Jaksa, M. B., Kuo, Y.L. and Airey, D. W. 2021b. Investigating the effectiveness of Rolling Dynamic Compaction (RDC) using Discrete Element Method (DEM). *Granular Matter*, 23, 1-21.

Chen, Y., Jaksa, M. B., Kuo, Y.L. and Airey, D. W. 2022. Experimental analysis of rolling dynamic compaction using transparent soils and particle image velocimetry. *Canadian Geotechnical Journal*, 59, 254-271.

Chung, O., Scott, B., Jaksa, M., Kuo, Y. and Airey, D. 2017. Physical modeling of rolling dynamic compaction. *Proceedings of the 19th Int. Conf. on Soil Mechanics and Geotechnical Engineering*, Seoul, Korea, Sept. 18–22, 905–908.

Clifford, J.M. 1980. The development and use of impact rollers in the construction of earthworks in southern Africa. CSIR Report 373. Pretoria, *South Africa: National Institute for Transport and Road Research*.

El-Gindy, M., Lescoe, R., O¨ Ijer, F., Johansson, I. and Trivedi, M. 2011. Soil modeling using FEA and SPH techniques for a tire-soil interaction. *International Design Engineering Technical Conferences and Computers and Information in Engineering Conference*. 793-802.

Gheshlaghi, F., Mardani, A. and Mohebbi, A. 2021. Investigating the effects of off-road vehicles on soil compaction using FEA-SPH simulation. *International Journal of Heavy Vehicle Systems*, 28, 455-466.

Gingold, R. A. and Monaghan, J. J. 1977. Smoothed particle hydrodynamics: theory and application to non-spherical stars. *Monthly notices of the royal astronomical society*, 181, 375-389.

Kuo, Y., Jaksa, M., Scott, B., Bradley, A., Power, C., Crisp, A. and Jiang, J. 2013. Assessing the effectiveness of rolling dynamic compaction. *Proceedings of the 18th International Conference on Soil Mechanics and Geotechnical Engineering*, Paris., vol. 2, pp. 1309–1312.

Liu, M. and Liu, G. 2010. Smoothed particle hydrodynamics (SPH): an overview and recent developments. *Archives of computational methods in engineering,* 17**,** 25-76.

LSTC 2018. LS-DYNA KEYWORD USER'S MANUAL. Livermore, California: Livermore Software Technology Corporation, ISBN: 0-9778540-2-7.

Lucy, L.B. 1977. A numerical approach to the testing of the fission hypothesis. *The astronomical journal,* 82**,** 1013-1024.

Pinard, M. 1999. Innovative developments in compaction technology using high energy impact compactors. *Proceedings 8th Australia New Zealand Conference on Geomechanics: Consolidating Knowledge*. Australian Geomechanics Society, 775.

Rajarathnam, P., Masoudian, M.S., Airey, D.W. and Jaksa, M.B. 2016. Model tests of rolling dynamic compaction. *Proc. 19th Southeast Asian Geotechnical Conf. and 2nd AGSSEA Conf. Kuala Lumpur Malaysia.*

Ranasinghe, R., Jaksa, M., Kuo, Y. and Pooya Nejad, F. 2017a. Application of artificial neural networks for predicting the impact of rolling dynamic compaction using dynamic cone penetrometer test results. *Journal of Rock Mechanics and Geotechnical Engineering,* 9**,** 340-349.

Ranasinghe, R., Jaksa, M., Nejad, F.P. and Kuo, Y. 2019. Prediction of the effectiveness of rolling dynamic compaction using artificial neural networks and cone penetration test data. *Chinese Journal of Rock Mechanics and Engineering,* 38**,** 153-170.

Ranasinghe, R.A.T.M., Jaksa, M.B., Pooya Nejad, F. and Kuo, Y.L. 2017b. Predicting the effectiveness of rolling dynamic compaction using genetic programming. *Proceedings of the Institution of Civil Engineers-Ground Improvement,* 170**,** 193-207.

Scott, B. and Jaksa, M. 2014. Evaluating rolling dynamic compaction of fill using CPT. *Proceedings of the 3rd International Symposium on Cone Penetration Testing*. 941-948.

Scott, B., Jaksa, M. and Mitchell, P. 2019. Ground response to rolling dynamic compaction. *Géotechnique Letters,* 9**,** 99-105.

Scott, B., Jaksa, M. and Syamsuddin, E. 2016. Verification of an impact rolling compaction trial using various in situ testing methods. *Proc. of 5th Int. Conf. on Geotechnical and Geophysical Site Characterisation*.

Scott, B.T., Jaksa, M.B., Mitchell and P.W. 2020. Influence of towing speed on effectiveness of rolling dynamic compaction. *Journal of Rock Mechanics and Geotechnical Engineering,* 12**,** 126-134.

Wang, W., Wu, Y., Wu, H., Yang, C. and Feng, Q. 2021. Numerical analysis of dynamic compaction using FEM-SPH coupling method. *Soil Dynamics and Earthquake Engineering,* 140**,** 106420.

Yao, Z., Zhou, C., Lin, Q., Yao, K., Satchithananthan, U., Lee, F. H., Tang, A. M., Jiang, H., Pan, Y., Wang, S. 2022. Effect of dynamic compaction by multi-point tamping on the densification of sandy soil. *Computers and Geotechnics,* 151**,** 104949.

Zhou, C., Jiang, H., Yao, Z., Li, H., Yang, C., Chen, L. and Geng, X. 2020. Evaluation of dynamic compaction to improve saturated foundation based on the fluid-solid coupled method with soil cap model. *Computers and Geotechnics,* 125**,** 103686.

Zhou, C., Yao, K., Rong, Y., Lee, F. H., Zhang, D., Jiang, H., Yang, C., Yao, Z. and Chen, L. 2022. Numerical investigation on zone of improvement for dynamic compaction of sandy ground with high groundwater table. *Acta Geotechnica***,** 1-15.